ACS APPLIED MATERIALS & INTERFACES

Research Article

www.acsami.org

Development of Inverted Organic Solar Cells with TiO_2 Interface Layer by Using Low-Temperature Atomic Layer Deposition

Zhenhua Lin,[†,‡] Changyun Jiang,*[,†] Chunxiang Zhu,*[,‡] and Jie Zhang[†]

[†]Institute of Materials Research and Engineering, A*STAR, 3 Research Link, Singapore 117602

[‡]Department of Electrical and Computer Engineering, National University of Singapore, 10 Kent Ridge Crescent, Singapore 119260

Supporting Information

ABSTRACT: Organic solar cells (OSCs) with inverted structure have attracted much attention in recent years because of their improved device air stability due to the use of stable materials for electrodes and interface layers. In this work, TiO_2 films, fabricated using low temperature (e.g., 130−170 °C) atomic layer deposition (ALD) on ITO substrates, are used as electron selective interface layers to investigate inverted OSCs. It is found that though the as-deposited TiO_2 films are high resistive due to the presence of oxygen defects, the defects can be significantly reduced by light soaking. PV cells with 15-nm-thick amorphous-TiO_2 layers fabricated at low temperature show better performance than those with poly crystal TiO_2 with same thickness deposited at 250 °C. The low temperature ALD-grown TiO_2 films are dense, stable and robust with capability of conformal coating on nanostructural surfaces, showing a promising interface layer for achieving air-stable plastic OSCs with roll-to-roll mass production potential.

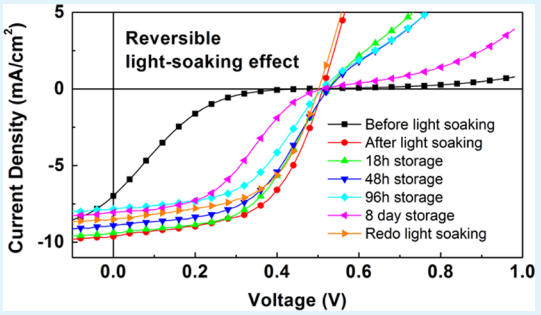

KEYWORDS: *low-temperature fabrication, TiO_2 thin film, atomic layer deposition, inverted structure, organic solar cells, light soaking*

1. INTRODUCTION

Organic solar cells (OSCs) have attracted much attention in recent years due to their unique advantages: capability of low-cost and large area fabrication process, and lightweight and mechanical flexibility using plastic substrates.[1−4] Bulk heterojunction of donor−acceptor has been proven a successful route toward solution processable OSCs with power conversion efficiency (PCE) up to ∼8%.[5] In most conventional OSCs, an acidic poly(3,4-ethyl-enedioxythiophene): poly(styrenesulfonate) (PEDOT:PSS) hole transport layer and low work function metal electrode such as aluminum or calcium are generally used. However, the strong acidic property of the PEDOT:PSS layer is detrimental to the indium−tin-oxide (ITO) electrode, and the low-work-function metal can be easily oxidized in air, both degrading devices' performance easily in air and leading to poor stability of the cells.[6−8]

One attempt to improve the air stability of OSCs is to use inverted structure,[9−12] where an n-type metal oxide film is used as the electron selective layer on ITO substrate (cathode) and a high work function metal such as silver or gold is used as the top anode. In the inverted structure, both the low-work-function metal and the interface of ITO/PEDOT:PSS can be avoided and thus enhances the air stability. One key challenge in making efficient inverted OSCs lies in the electron selective buffer layer: it should work as a high conductive path for efficient electron extraction while exhibit good hole blocking capability. A number of works have been carried out in inverted OSCs using TiO_2 film as electron selective layer, owing to its superior air stability as compared to other semiconductor oxides. The synthesis of TiO_2 has been investigated a lot,[13−19] and there are several methods commonly used to fabricate a compact TiO_2 thin film, including sol−gel (or suspension) solution processing,[17,18] and spray pyrolysis.[19] Spray pyrolysis usually employs a high-temperature (>250 °C) process for decomposition of titanium oxide precursors, which may be not suitable for low-cost plastic substrates. The sol−gel solution processing methods have demonstrated promising potential for low temperature and roll-to-roll fabrication of TiO_x thin film for OSCs. However, it has its limitations in precisely controlling the thickness and uniformity of the ultrathin TiO_x film over large area and its poor conformal coating capability on nanostructured surfaces.[20−22] Low-temperature atomic layer deposition (ALD) seems more suitable for fabrication of compact TiO_2 film due to its capability in achieving uniform, dense and highly conformal films on 2D and 3D surfaces, and on plastic substrates.[23] However, there are very few reports on inverted OSCs using ALD-processed TiO_2 film as the electron selective layer. Kang et al. ever reported an efficient inverted OSC fabricated by using nanocrystalline TiO_2 film deposited by ALD at 220 °C.[24] However, this deposition temperature is too high for commonly used plastic substrates such as polyethylene terephthalate (PET) or polyethylene naphthalate (PEN). In a recent study of using TiO_2/ZnO selection layer for inverted

Received: October 8, 2012
Accepted: January 21, 2013
Published: January 21, 2013

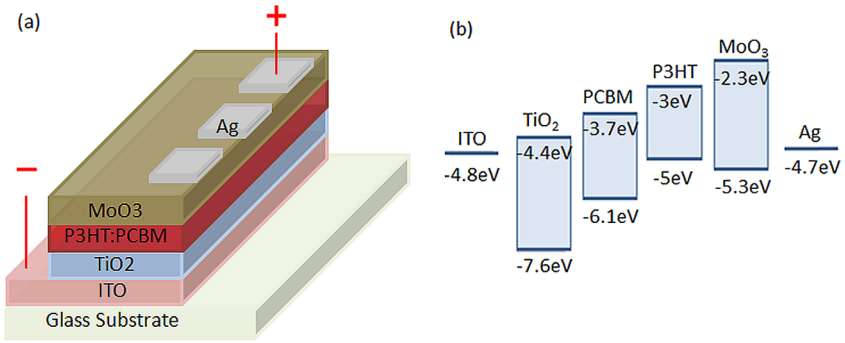

Figure 1. (a) Schematic device structure and (b) the energy band diagram of the inverted organic solar cells.

OSC, ALD-processed TiO_2 is only used as a surface modification on ZnO film because of its high resistance.[25]

In this report, inverted OSC devices using low-temperature ALD-processed TiO_2 films on ITO as the cathodes were studied. The effects of ALD temperature, TiO_2 film thickness, and light-soaking treatment on cell performance were investigated. It was found that a short time light soaking significantly improves the device performance by reducing the defects caused from atmosphere-gas incorporated in the TiO_2 layer. With an ultrathin (~15 nm) amorphous TiO_2 layer fabricated by ALD at low temperature (e.g., 130−170 °C), efficient inverted OSC devices based on poly(3-hexylthiophene) (P3HT) and 1-(3-methoxycarbonyl)-propyl-1-phenyl-(6,6)C61 (PCBM) blend were achieved. The low-temperature ALD-fabricated TiO_2 film on ITO substrate is stable and robust, and the process is compatible with low-cost plastic substrates, showing a promising manufacturing potential for plastic OPVs.

2. EXPERIMENTAL SECTION

ITO-coated glass substrates were cleaned by a routine solvent ultrasonic cleaning, sequentially with detergent, deionized water, acetone, and isopropanol in an ultrasonic bath for 15 min each. After that, TiO_2 layer was deposited on the top of ITO layer by ALD. For the ALD deposition, the precursors used were water (H_2O) and titanium tetrachloride ($TiCl_4$). The pulse time for each reactant was set to 0.5 s, and nitrogen was used as a purge and carrier gas with the flow rate of 50 sccm and the purging time was set to 30 s. Different deposition temperatures of 130, 150, 170, and 250 °C were used for the growths, and the layer thickness was controlled by the number of growth cycles. Following that, an active layer was deposited on top of the TiO_2 layer by spin-coating a solution of the P3HT (Rieke Metals) and PCBM (Nano-C) blend with a weight ratio of 1:0.8 in 1, 2-dicholorobenzen (40 mg/mL) at 500 rpm for 120 s in N_2 environment. The active layers were dried on a hot plate at 80 °C for 2 h and then annealed at 160 °C for 10 min. Finally, a MoO_3 layer (8.5 nm) and an Ag layer (100 nm) were deposited by using vacuum thermal evaporation. A metal shadow mask was used for the Ag deposition to define the device area of 12 mm^2. Figure 1a and b illustrate the schematic device structure and the band diagram of the inverted OSCs, respectively. The current density−voltage (J−V) characteristics of the devices were measured using a Keithley 2400 parameter analyzer in the dark and under a simulated light (AM 1.5G) with intensity of 100 mW/cm^2. The TiO_2 films were prepared by Azimuth atomic layer deposition system. Film properties of the ALD-deposited TiO_2 were characterized by 2D X-ray diffraction (XRD) (Bruker-AXS D8-GADDS), X-ray photoelectron spectroscopy (XPS) (VG ESCALAB-220i XL), and field emission scanning electron microscopy (FESEM) (JEOL JSM6700F). The transmittance of the TiO_2 films (on ITO/glass) was characterized using an UV-3600 Shimadzu UV−vis−NIR Spectrophotometer. The thermal evaporation system used was EL3600 OLED deposition system (Advanced Neotech Systems).

3. RESULTS AND DISCUSSION

Figure 2 shows the XRD patterns of TiO_2 thin films deposited by ALD at 130, 150, 170, and 250 °C on Si wafer substrate. It

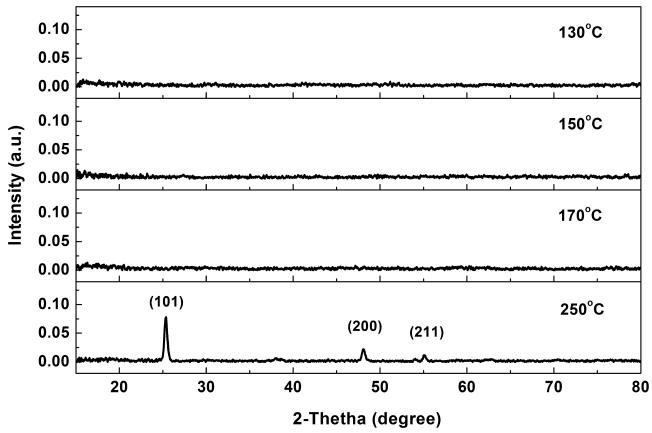

Figure 2. XRD patterns of TiO_2 films grown by ALD at 130, 150, 170, and 250 °C, respectively.

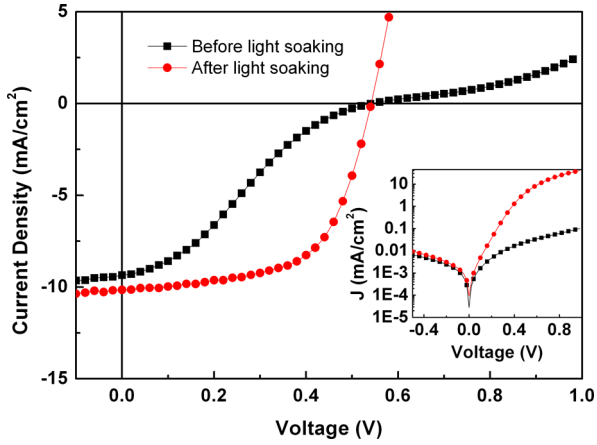

Figure 3. J−V curves measured under illumination of a cell before and after light soaking. Inset: the dark J−V curves before (black squares) and after (red circles) light soaking.

can be seen that the film deposited at 250 °C shows clearly the characteristic (101) and (200) diffraction peaks of anatase TiO_2 crystalline phase, whereas no diffraction peaks originated from crystalline TiO_2 are observed from the film deposited at 130,

dx.doi.org/10.1021/am302252p | ACS Appl. Mater. Interfaces 2013, 5, 713−718

Table 1. Values of Photovoltaic Performance Parameters of Inverted OSCs with Different Thickness TiO_2 Layers Grown at 170 °C by ALD Process (under simulated illumination of 100 mW/cm^2 AM 1.5G)[a]

TiO_2 thickness (nm)	J_{sc} (mA/cm^2)	V_{oc} (V)	FF	η (%)	R_s (Ω/cm^2)	R_{sh} (Ω/cm^2)	remark
10	7.08	0.46	0.20	0.65	99	120	as-fabricated
	7.59	0.49	0.44	1.63	7.68	177	after light soaking
12	8.29	0.49	0.19	0.75	904	102	as-fabricated
	8.91	0.53	0.58	2.71	9.1	398	after light soaking
15	9.35	0.54	0.26	1.33	399	418	as-fabricated
	10.16	0.54	0.60	3.31	5.58	310	after light soaking
17	8.52	0.53	0.19	0.88	461	89.1	as-fabricated
	9.42	0.53	0.56	2.83	8.4	338	after light soaking
20	4.82	0.51	0.19	0.27	138	45.2	as-fabricated
	8.60	0.53	0.53	2.43	5.8	376	after light soaking

[a]Devices were measured as-fabricated and after light soaking (5 min simulated illumination).

Table 2. Values of Photovoltaic Performance Parameters of Inverted OSCs with 15 nm Thick TiO_2 Layer Grown at Different Temperatures by ALD Process (under simulated illumination of 100 mW/cm^2 AM 1.5G)[a]

deposition temperature (°C)	J_{sc} (mA/cm^2)	V_{oc} (V)	FF	η (%)	R_s (Ω/cm^2)	R_{sh} (Ω/cm^2)	remark
130	4.49	0.52	0.10	0.23	147	432	as-fabricated
	8.43	0.53	0.59	2.65	4.94	967	after light soaking
150	4.27	0.42	0.12	0.22	160	456	as-fabricated
	8.50	0.54	0.59	2.72	4.39	627	after light soaking
170	9.35	0.54	0.26	1.33	399	418	as-fabricated
	10.16	0.54	0.60	3.31	5.58	310	after light soaking
250	7.84	0.52	0.26	1.05	289	551	as-fabricated
	8.75	0.52	0.56	2.59	7.84	338	after light soaking

[a]Devices were measured as-fabricated and after light soaking (5 min simulated illumination).

150, and 170 °C, indicating that the TiO_2 film deposited by ALD at 170 °C or below is amorphous in nature. The Ti/O ratio calculated from the XPS measurement (see the Supporting Information, Figure S1) is about 1:2 for all the samples.

Inverted cells using TiO_2 films with different thicknesses produced on ITO by ALD at 170 °C were fabricated. It was found that the $J-V$ curves measured for all these cells as fabricated show a pronounced S-shape and the S-shape can be removed after a short time (typically 5−10 min) light soaking (under illumination, AM1.5G, 100 mW/cm^2). Figure 3 shows one example of the $J-V$ curves measured for a cell as fabricated and after light soaking. Table 1 shows the values of photovoltaic performance parameters measured as fabricated and after light soaking of the cells with different TiO_2 thicknesses from 10, 12, 15, 17, to 20 nm. From the data of measurements after light soaking, it can be seen that with the increase of the TiO_2 film thickness, the open circuit voltage (V_{oc}), short circuit current density (J_{sc}), fill factor (FF), and PCE all increase first and reach to their maximum values (V_{oc} = 0.54 V, J_{sc} = 10.10 mA/cm^2, FF = 0.60 and PCE = 3.31%) at 15 nm thickness, and then decrease with further increase of the TiO_2 thickness. The lower cell performance at thinner (10−12 nm) and thicker (17−20 nm) TiO_2 thickness is mostly because that a relatively thinner layer of TiO_2 will increase the hole leakage through the TiO_2 layer leading to an increased recombination of electrons and holes and hence a reduction on V_{oc}, FF, and J_{sc}; whereas a relatively thicker amorphous TiO_2 layer will increase the resistance for electron transport and cause the electrons more difficult to be collected at the cathode, and hence a reduction in the FF and J_{sc}. The similar trend on TiO_2 thicknesses was also observed in the performance data without light soaking (measurements as fabricated). Meanwhile, comparing measurements as-fabricated with those after light soaking, the cell performance was significantly increased after light soaking because of the largely decreased series resistance. The series resistances (R_s) of the devices with light soaking decreased at least tens of times as compared with those of the devices without light soaking for all the devices with different TiO_2 thicknesses, which causes both J_{sc} and FF increased. Taking the performance of the device with 15 nm thick TiO_2 film as an example, after light soaking, the R_s decreases from 399 to 5.58 Ω/cm^2, the J_{sc} increases form 9.35 to 10.16 mA/cm^2 and the FF increases from 0.26 to 0.60, which makes the PCE increased by 149%, from 1.33 to 3.31%.

The effect of deposition temperature of TiO_2 has also been investigated. Inverted solar cells with 15 nm thick TiO_2 layer deposited by ALD at different temperatures (130, 150, 170, and 250 °C) were fabricated, and the values of photovoltaic performance parameters of these cells are presented in Table 2, where the measurements were also done as fabricated and after light soaking. From the XRD pattern shown in Figure 2, it can be seen that the TiO_2 film is amorphous in nature when the deposition temperature is 170 °C or below, and the film becomes poly crystal when the temperature is 250 °C. It can be found that when the TiO_2 film is in amorphous phase, with the increase of the TiO_2-deposition temperature from 130 to 170 °C, the V_{oc} and FF are nearly the same, and only J_{sc} increases and reaches a maximum value of 10.16 mA/cm^2 at 170 °C. The considerable change solely in J_{sc} is usually arisen from the active layer (P3HT:PCBM) with changes in morphology or optical coupling. This is possible because the TiO_2 layers fabricated at different temperature have different surface and optical properties, which usually affects the morphology and light absorption in the active layer.[26] Figure 4 shows the surface SEM images and transmittance spectra of these TiO_2 films with

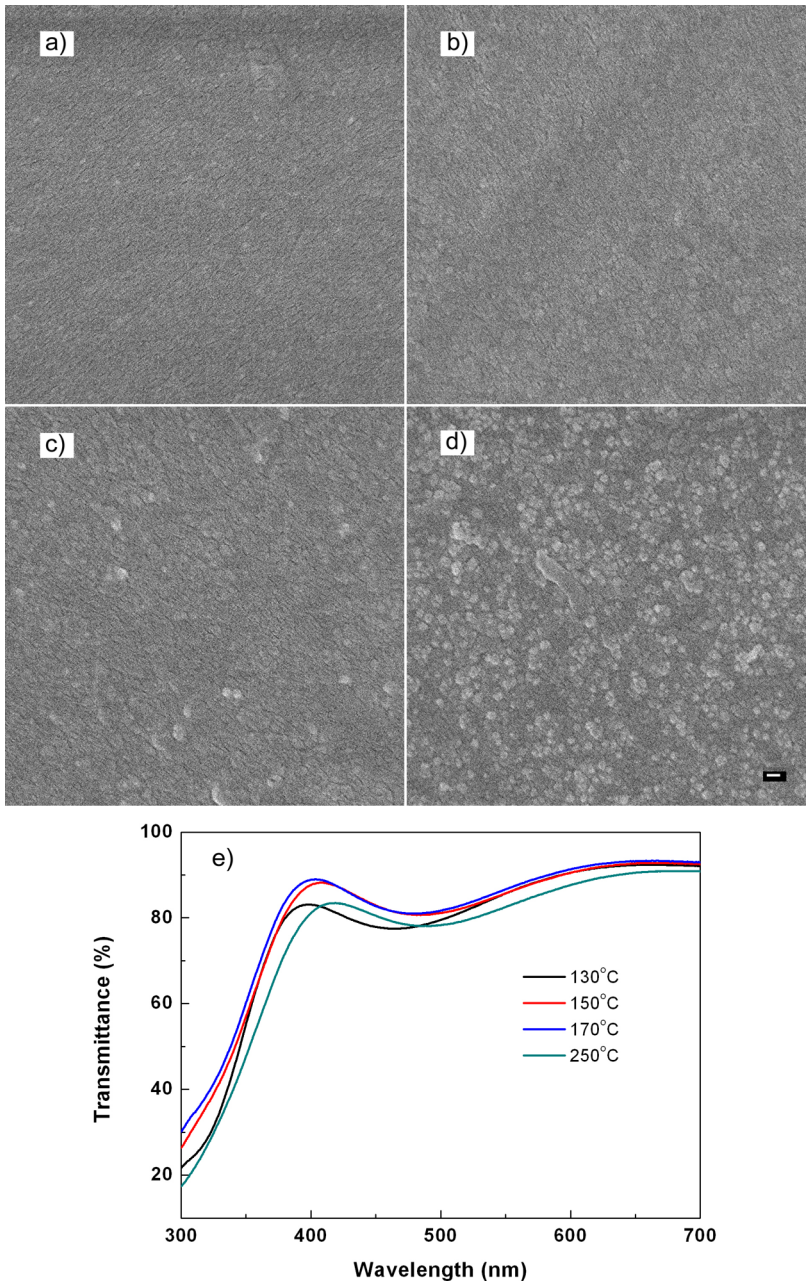

Figure 4. Surface FESEM images of TiO_2 films deposited at (a) 130, (b) 150, (c) 170, and (d) 250 °C (scale bar: 100 nm), and (e) the optical transmittance of these films.

different deposition temperatures. The SEM images (Figure 4a–d) show that the roughness of TiO_2 films increases with the increase in the deposition temperature because of the growing of the grain size on the film, which becomes pronounced in the TiO_2 film deposited at 250 °C. From Figure 4e, it shows that the transmittances are different in these TiO_2 films; with the 170 °C-deposited film has the highest transmittance in the wavelength range of 300–700 nm. However, when the deposition temperature is further increased to 250 °C, it results in a poly crystal TiO_2 layer, and the cell has decreased V_{oc} and FF as compared to the other cells with amorphous TiO_2 films as shown in Table 2. The most possible reason is that the ultrathin thickness (15 nm) is not thick enough for the poly crystal TiO_2 film to fully block the holes, since there are grain boundaries formed in the film (see Figure 4d), which makes holes easier to be collected by the cathode and leads to a higher recombination of electrons and holes and hence a reduction of V_{oc} and FF.

Nevertheless, the better performance of the cells based on 15 nm amorphous TiO_2 layers fabricated at low temperature (130–170 °C) as compared to that of the cell with the 15 nm poly crystal TiO_2 layer demonstrates that low temperature ALD processed ultrathin and dense TiO_2 layer is promising for use to achieve high performance and stable OSCs on plastic substrate. Moreover, the stable and robust ALD-produced TiO_2 film makes it possible to integrate the TiO_2 films on ITO plastic substrates for easier processing and distribution of the film products, which will benefit the roll-to-roll mass production of plastic OSCs.

For our case, the observed S-shape together with the high series resistance (see Table 1, measurements as fabricated) is mostly because of the low electrical conductivity of these TiO_2

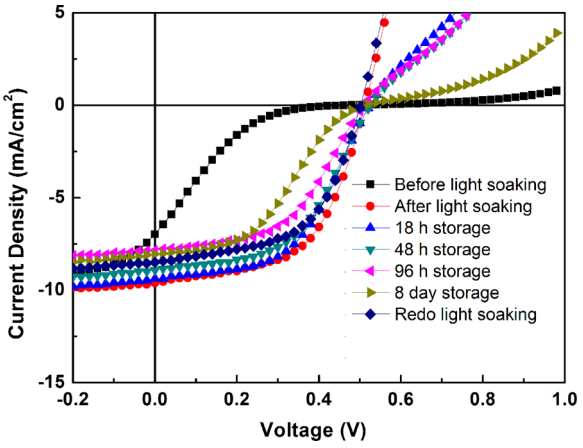

Figure 5. $J-V$ curves of a cell measured after different storage time in N_2-filled glovebox.

layers. The S-shape is removed and the series resistance of the device is significantly decreased after light soaking, indicating that light illumination changed the electrical properties of the TiO_2 film. It is usually thought that high density surface state is produced on TiO_2 upon UV-light illumination, which may result in improved electron transport.[27] The surface states could be from oxygen vacancy or Ti^{3+} states induced by the photoreaction under light soaking.[28,29]

The change in the S-shape by light soaking is found reversible after storing the cell inside glovebox (without illumination) for a period of time. It is observed from Figure 5 that, for the device after light soaking and stored in glovebox, the S-shape is returned bit by bit with the increase in the storage time, from 18, 48, and 96 h to 8 days. Furthermore, when the device was placed under one more light soaking, the S-shape can be removed again.

To further investigate the cause for the S-shape, we put the S-shape removed devices stored in three different environments of air ambient (drybox), N_2-filled glovebox and high vacuum (8×10^{-7} Torr) separately, and measured the $J-V$ characteristics before and after the storages (as shown in Figure 6). Figure 6a shows that there is an obvious S-shape appeared in the $J-V$ curve of the device stored in air ambient after only 3 h. Moreover, there is little S-shape appeared in the $J-V$ curve of the device stored in the glovebox even after 4 h, as shown in Figure 6b. Furthermore, there is no S-shape appeared in the

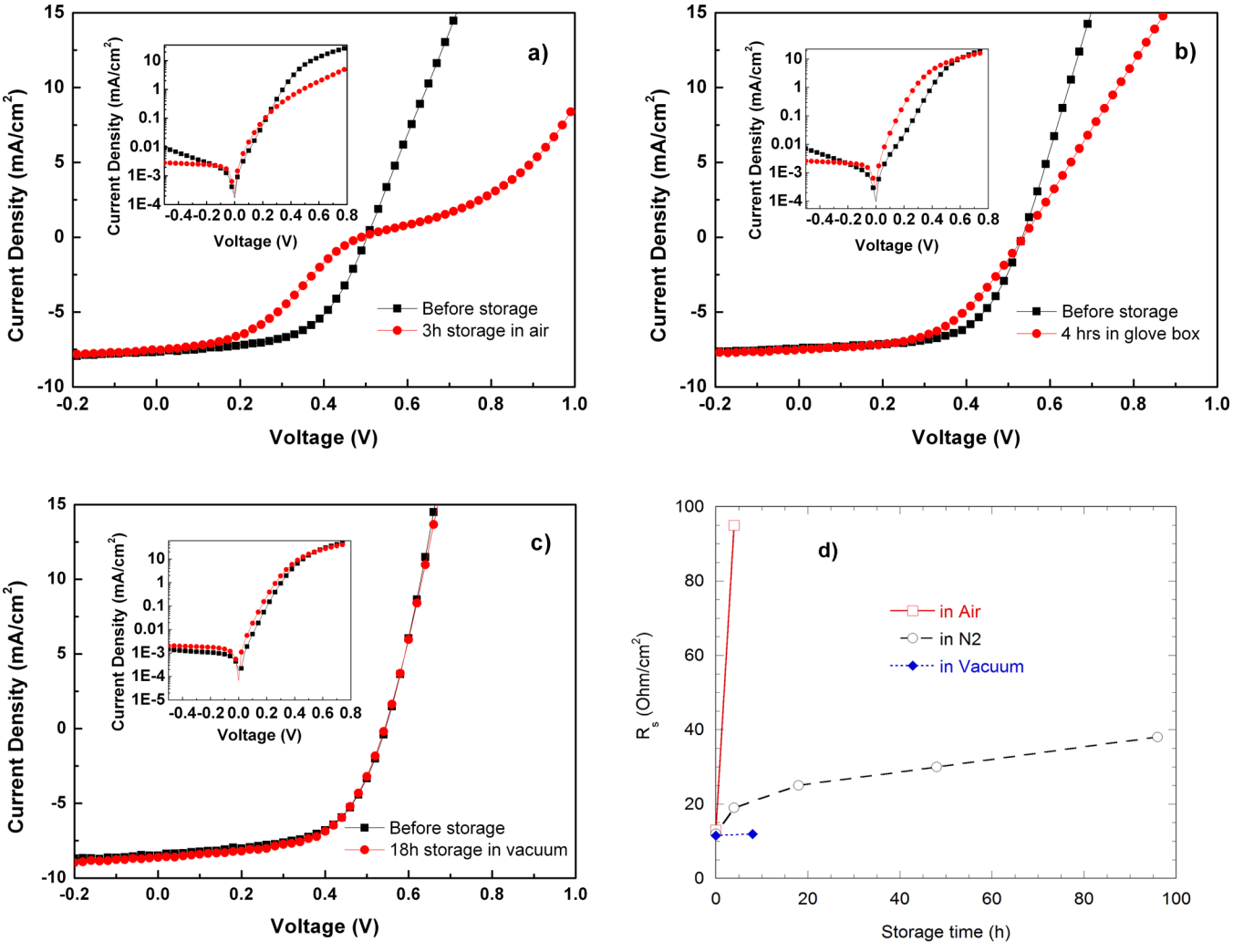

Figure 6. $J-V$ curves measured for devices before and after storage (a) in air ambient for 3 h, (b) in glovebox for 4 h, (c) in high vacuum for 18 h (light soaking for 5 min was conducted for each cell before the storage), and the change of the series resistance R_s with storage times (d). Insets of a, b, and c are the corresponding dark $J-V$ curves before (black line) and after (red line) storages.

dx.doi.org/10.1021/am302252p | ACS Appl. Mater. Interfaces 2013, 5, 713−718

device that stored in high vacuum ambient for even 18 h (Figure.6c). Figure 6d shows the changes of the series resistance R_s with storage time in these three conditions. It can be seen that R_s rises very quickly in air ambient, whereas it shows much slower changes in N2 and vacuum conditions. The different behaviors of S-shape with different storage ambiences can be explained by different amounts of oxygen: the amount of oxygen contained in air ambient is much more than those contained in glovebox and high vacuum, so it will be more quickly for the TiO_2 layer to adsorb oxygen in air ambient. Despite the mechanism of how the TiO_2 layer changes after oxygen adsorption being unclear, it is reasonable to think that there are surface Ti^{3+} states returning to Ti^{4+} states on O_2 adsorption, which causes the conductivity of the TiO_2 film to decrease and the S-shape to return back. Further investigation on the mechanism of the light soaking effect is on going. The much improved stability observed in the devices stored in the high vacuum suggests that the S-shape can also be permanently removed by proper encapsulation of the devices to prohibit the oxygen and water contamination, which needs further investigation.

4. SUMMARY

In summary, ALD-grown TiO_2 film was used as the electron selective layer in inverted OCSs. The high resistance of TiO_2 film is due to the presence of oxygen defects in the film, while after several minutes light soaking the defects were removed leading to the increase of the TiO_2 film conductivity and significant improvement of the cell performance. By using the ultrathin (~15 nm) amorphous TiO_2 film fabricated by ALD at low temperature (130−170 °C), efficient inverted polymer solar cells are demonstrated. The stable and robust TiO_2 film with low temperature process has the potential to enable a roll-to-roll mass production and distribution of TiO_2 films coated on ITO plastic substrates, demonstrating a promising manufacturing potential for air-stable plastic solar cells.

■ ASSOCIATED CONTENT

Supporting Information

XPS measurements for the TiO_2 films deposited at different temperature and the incident photon-to-electron conversion efficiency (IPCE) for the cell with 15 nm TiO_2 layer deposited at 170 °C. This material is available free of charge via the Internet at http://pubs.acs.org/.

■ AUTHOR INFORMATION

Corresponding Author

*E-mail: jiangc@imre.a-star.edu.sg (C.J.); elezhucx@nus.edu.sg (C.Z.).

Notes

The authors declare no competing financial interest.

■ ACKNOWLEDGMENTS

This work is sponsored by SERC (Science and Engineering Research Council) of A*STAR (Agency of Science and Technology Research) and IMRE (Institute of Material Research and Engineering IMRE/11-1P0508) in Singapore.

■ REFERENCES

(1) Baek, W. H.; Seo, I.; Yoon, T. S.; Lee, H. H.; Yun, C. M.; Kim, Y. S. *Sol. Energy Mater. Sol. Cells* **2009**, *93*, 1587−1591.
(2) Wang, J. C.; Weng, W.-T.; Tsai, M.-Y.; Lee, M.-K.; Horng, S.-F.; Perng, T.-P.; Kei, C.-C.; Yuc, C.-C.; Mengd, H.-F. J. *Mater. Chem.* **2010**, *20*, 862−866.
(3) Zhang, F.; Xu, X.; Tang, W.; Zhang, J.; Zhuo, Z.; Wang, J.; Wanga, J.; Xu, Z.; Wanga, Y. *Sol. Energy Mater. Sol. Cells* **2011**, *95*, 2758−2761.
(4) Huang, J.-S.; Chou, C.-Y.; Liu, M.-Y.; Tsai, K.-H.; Lin, W.-H.; Lin, C.-F. *Org. Electron.* **2009**, *10*, 1060−1065.
(5) Liang, Y.; Xu, Z.; Xia, J.; Tsai, S.-T.; Wu, Y.; Li, G.; Ray, C.; Yu, L. *Adv. Mater.* **2010**, *22* (20), E135−E138.
(6) de Jong, M. P.; van Ijzendoom, L. J.; de Voigt, M. J. A. *Appl. Phys. Lett.* **2000**, *77*, 2255−2257.
(7) Greczynski, G.; Kugler, T.; Keil, M.; Osikowicz, W.; Fahlman, M.; Salaneck, W. R. *J. Electron spectrosc. Relat. Phenom.* **2001**, *121*, 1−17.
(8) Kyaw, A. K. K.; Sun, X. W.; Jiang, C. Y.; Lo, G. Q.; Zhao, D. W.; Kwong, D. L. *Appl. Phys. Lett.* **2008**, *93*, 221107.
(9) Hau, S. K.; Yip, H.-L.; Baek, N. S.; Zou, J.; O'Malley, K.; Jen, A. K.-Y. *Appl. Phys. Lett.* **2008**, *92*, 253301.
(10) Chen, L. M.; Hong, Z.; Li, G.; Yang, Y. *Adv. Mater.* **2009**, *21*, 1434−1449.
(11) Xu, Z.; Chen, L. M.; Yang, G. W.; Huang, C. H.; Hou, J.; Wu, Y.; Li, G.; Hsu, C. S.; Yang, Y. *Adv. Funct. Mater.* **2009**, *19*, 1227−1234.
(12) Hau, S. K.; Yip, H.-L.; Jen, A. K.-Y. *Polym. Rev.* **2010**, *50*, 474−510.
(13) Violi, I. L.; Perez, M. D.; Fuertes, M. C.; Soler-Illia, G. J. A. A. *ACS Appl. Mater. Interfaces* **2012**, *4*, 4320−4330.
(14) Nilsson, E.; Sakamoto, Y.; Palmqvist, A. E. C. *Chem. Mater.* **2011**, *23*, 2781−2785.
(15) Rawolle, M.; Braden, E. V.; Niedermeier, M. A.; Magerl, D.; Sarkar, K.; Fröschl, T.; Hüsing, N.; Perlich, J.; Müller-Buschbaum, P. *ChemPhysChem* **2012**, *13*, 2412−2417.
(16) Xie, J. Y.; Wang, H.; Bai, H. D.; Yang, P.; Shi, M. X.; Guo, P.; Wang, C.; Yang, W. T.; Song, H. H. *ACS Appl. Mater. Interfaces* **2012**, *4*, 2891−2896.
(17) Waldauf, C.; Morana, M.; Denk, P.; Schilinsky, P.; Coakley, K.; Choulis, S. A.; Brabec, C. J. *Appl. Phys. Lett.* **2006**, *89*, 233517.
(18) Kim, J. Y.; Kim, S. H.; Lee, H.-H.; Lee, K.; Ma, W.; Gong, X.; Heeger, A. J. *Adv. Mater.* **2006**, *18*, 572−576.
(19) Sun, H.; Weickert, J.; Hesse, H. C.; Schmidt-Mende, L. *Sol. Energy Mater. Sol. Cells* **2011**, *95*, 3450−3454.
(20) Rim, S. B.; Zhao, S.; Scully, S. R.; McGehee, M. D.; Peumans, P. *Appl. Phys. Lett.* **2007**, *91*, 243501.
(21) He, L.; Lai, D.; Wang, H.; Jiang, C.; Rusli. *Small* **2012**, *8*, 1664−1668.
(22) Müller-Meskamp, L.; Kim, Y. H.; Roch, T.; Hofmann, S.; Scholz, R.; Eckardt, S.; Leo, K.; Lasagni, A. F. *Adv. Mater.* **2012**, *24*, 906−910.
(23) Aarik, J.; Aidla, A.; Mändar, H.; Uustare, T. *Appl. Surf. Sci.* **2001**, *172*, 148−158.
(24) Kang, Y.-J.; Kim, C. S.; Kwon, S.-H.; Kang, J. W. *37th IEEE Photovoltaic Specialists Conference*; Seattle, June 19−24, 2011 ; IEEE: Piscataway, NJ, 2011; pp 001165−001166.
(25) Seo, H. O.; Park, S. Y.; Shim, W. H.; Kim, K. D.; Lee, K. H.; Jo, M. Y.; Kim, J. H.; Lee, E.; Kim, D. W.; Kim, Y. D.; Lim, D. C. *J. Phys. Chem. C* **2011**, *115*, 21517−21520.
(26) Campoy-Quiles, M.; Ferenczi, T.; Agostinelli, T.; Etchegoin, P. G.; Kim, Y.; Anthopoulos, T. D.; Stavrinou, P. N.; Bradley, D. D. C.; Nelson, J. *Nat. Mater.* **2008**, *7*, 158−164.
(27) Gregg, B. A.; Chen, S. G.; Ferrere, S. *J. Phys. Chem. B* **2003**, *107*, 3019−3029.
(28) Wang, R.; Hashimoto, K.; Fujishima, A.; Chikuni, M.; Kojima, E.; Kitamura, A.; Shimohigoshi, M.; Watanabe, T. *Adv. Mater.* **1998**, *10*, 135−138.
(29) Komaguchi, K.; Maruoka, T.; Nakano, H.; Imae, I.; Ooyama, Y.; Harima, Y. *J. Phys. Chem. C* **2009**, *113*, 1160−1163.